Thermal Rate Constants for $SiH_4 \rightleftarrows SiH_3+H$ and $CH_4 \rightleftarrows CH_3+H$ by Canonical Variational Transition State Theory#

Junko TAKAHASHI,* Takamasa MOMOSE, and Tadamasa SHIDA
Department of Chemistry, Faculty of Science, Kyoto University, Kyoto 606-01
(Received August 16, 1993)

The thermal rate constants for $SiH_4 \rightleftarrows SiH_3+H$ and $CH_4 \rightleftarrows CH_3+H$ are calculated by the Canonical Variational Transition State Theory (CVTST). The minimum energy path potential and the deformation path potential along the reaction coordinate are calculated by the MCSCF-CI and UHF methods, respectively. The transitional bending mode which connects the bending vibrations of the parent molecules with the translational and rotational motions of the products of the dissociation is treated in terms of a two-dimensional quantum hindered rotor. The saddle points and the CVTST rate constants are determined by the maximum free energy criterion. Comparative discussions are made for the two systems. The calculated association rate constants for the SiH_4 system are 8.4×10^{10} l mol^{-1} s^{-1} at 300 K and 12.5×10^{10} l mol^{-1} s^{-1} at 2000 K, while those for the CH_4 system are 12.5×10^{10} l mol^{-1} s^{-1} and 18.6×10^{10} l mol^{-1} s^{-1} at the two temperatures. At all the temperatures studied the rate constant of the former system is smaller by 30—35% than the latter. The dissociation rate constants are evaluated to be 7.2×10^{5} s^{-1} at 2000 K and 1.2×10^{9} s^{-1} at 3000 K for the SiH_4 system, while the constant for the CH_4 system at 2000 K is about one order of magnitude smaller. This difference diminishes at higher temperatures. The results are also compared with experimental and other theoretical studies.

Chemical vapor deposition (CVD) of silane is an important technique in the production of silicon thin films used for microelectronics and solar-cell industries. CVD processes involve the following steps;[1—3] 1) decomposition processes of the reactor molecules in the gas phase, 2) mass transport processes of radicals onto the substrate (with cluster formation and/or polymerization), 3) surface reaction processes on the substrate. Although the elucidation of the elementary CVD processes is definitely needed, the experimental approach is difficult due to the complexity of the overall processes. Under the circumstance predictive theoretical studies of elementary processes of silane play a significant role.

The major primary processes in the gas phase are the decomposition of SiH_4 to SiH_3+H and SiH_2+H_2. From the experimental and theoretical studies the reaction enthalpies for these reactions are estimated to be about 90 and 60 kcal mol^{-1}, respectively.[2] The latter reaction is considered as the main channel of the decomposition process of SiH_4, but the former also becomes significant at higher temperatures. R. Viswanathan et al. calculated the microcanonical rate constant of the decomposition of SiH_4 by a quasiclassical trajectory method.[3] They obtained the total thermal rate constant of both channels by applying the results of the trajectory calculation to the RRK theory.

In the present work we focus on the unimolecular dissociation and association in Eq. 1 whose experimental thermal rate constants are scarcely available.

$$SiH_4 \rightleftarrows SiH_3 + H. \quad (1)$$

The theoretical study of the processes in Eq. 1 is also of interest from the viewpoint of comparison with the well studied processes in Eq. 2.

$$CH_4 \rightleftarrows CH_3 + H. \quad (2)$$

The experimental rate constant of the association in Eq. 2 was reported by J. Cheng et al., T. J. Sworski et al., and R. Patrick et al.[4—6] Theoretically also the association rate constant of Eq. 2 was calculated by various methods; W. L. Hase and R. J. Duchovic and J. F. LeBlanc et al. calculated the rate constant by the canonical variational transition state theory (CVTST) and the classical and quasiclassical trajectory methods[8—11] on the basis of an analytic model potential developed by Duchovic, Hase, and Schlegel (DHS).[7] W. L. Hase et al. and E. E. Aubanel et al. employed the CVTST and the flexible transition state theory in combination with the modified DHS potential.[12,13] X. Hu et al. also used the CVTST and the classical trajectory method with another modified DHS potential.[14] Finally, a statistical adiabatic channel model was used by C. J. Cobos et al. for the calculation.[15]

Since these previous studies indicate that there is no potential energy barrier for the reaction in Eq. 2, the rate constants need to be calculated by a variational transition state theory. In the present work, we have employed CVTST, which gives the saddle point by the maximum free energy criterion.[16] The CVTST method gives us thermally averaged rate constants that are directly comparable with the experimental result. The accuracy of the rate constant depends critically on the accuracy of the potential energy surface which is determined by ab initio MO calculations in the present work.

The multidimensional potential energy surface is reduced to that characterized by the minimum energy path and the deformation path potentials. The min-

#This paper is dedicated to the memory of the late Professor Hiroshi Kato.

imum energy path potential is determined as the potential energy at the optimized geometry for a given value of the reaction coordinate R, which is taken to be the distance between the Si or C atom and the incoming or the dissociating H atom. The deformation potential is described in terms of the vibrational potential in the vicinity of the energy minimum.[7)]

The vibrational freedoms of the methane system are known to be classified into two groups according to the behavior along the minimum energy path;[9—14)] the first group includes the normal vibrations of CH_4 in the equilibrium geometry which correlate smoothly with those of CH_3. The second group comprises the doubly degenerate bending vibrations of CH_4 which correlate to the translation and rotation of the dissociation fragments, i.e., CH_3 and H. In the transition state the behavior of the latter group is described as a hindered internal rotation of the incoming or the dissociating H atom in the angular deformation potential.[7)] In the present work we treated the vibrations of the first group as harmonic and those of the second group as a two-dimensional quantum hindered rotor.[17)]

In the following the method and result of ab initio MO calculations for the potential energy surfaces are described along with the vibrational analysis by both the harmonic and hindered rotor treatments. Then, the method and result of the CVTST calculation for the rate constant are followed. Comparative discussions are made for the silane and methane systems before the final conclusion.

Potential Energy Surface

Method of Calculation. We have calculated the potential energy surfaces for $SiH_4 \rightleftarrows SiH_3+H$ and $CH_4 \rightleftarrows CH_3+H$ along the reaction coordinate R which is chosen to be the distance between the Si or C atom and the counterpart H atom. The potential energy surface near the reaction coordinate is described in the following form;[18)]

$$W(R,\{q\}) = V(R) + \frac{1}{2}\sum_{ij} f_{ij}(R)\Delta q_i \Delta q_j, \qquad (3)$$

where $V(R)$ is the minimum energy path potential which is defined as the potential energy at the optimized geometry for a given value of R. The geometry optimization is performed by using the analytic gradient method for the UHF wave function with the C_{3v} symmetry being kept for a given R. The optimized variables are the length r and the angle ϕ in Fig. 1. The potential energy $V(R)$ is calculated for each optimized geometry by the MR-SD-CI procedure following the MCSCF procedure described below. The symbol Δq_i represents the displacement of the internal coordinate which is a function of R. The force constant f_{ij} is also a function of R. Here, the number of the internal coordinates is eight excepting R. The force constants are calculated by the numerical differentiation of the energy gradient with the

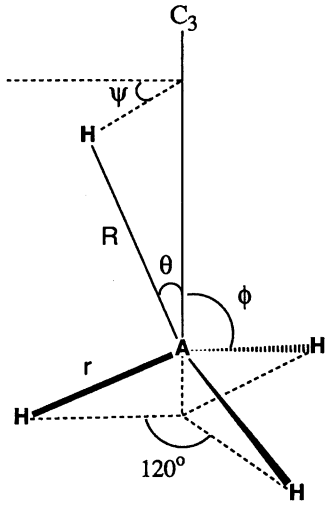

Fig. 1. The coordinate system for $SiH_3\cdots H$ or $CH_3\cdots H$. The center atom is Si or C. R is the reaction coordinate. The length r and angle ϕ determine the optimized geometry for given R. The angle θ and ψ describe the motion of the hindered rotor.

UHF wave function. They are calculated first in the Cartesian coordinate system and then transformed into the internal coordinate system.

The basis set is the Huzinaga–Dunning DZ basis plus polarization functions (DZP): (12s8p1d/4s1p)/[6s4p1d/2s1p] for SiH_4 and (9s5p1d/4s1p)/[4s2p1d/2s1p] for CH_4. The exponents of the d-polarization function are chosen to be 0.3247 for the Si-atom and 0.75 for the C-atom and the exponent of the p-polarization function of the H-atom to be 1.0.

For the MCSCF wave function the CAS-type configurations with eight electrons in the eight active orbitals $[(4a_1)(2e)(5a_1)(6a_1^*)(3e^*)(7a_1^*)]$ are used for SiH_4, and $[(2a_1)(1e)(3a_1)(4a_1^*)(5a_1^*)(2e^*)]$ for CH_4. The total number of the configuration is 1764 in the C_{3v} symmetry.

For the CI wave function the natural orbitals obtained by the MCSCF calculation are used as one-particle basis functions, and all the single and the double excitations from the following three reference configurations with the CI coefficients larger than 0.1 at a large R are included; $[(4a_1)^2(2e)^4(5a_1)^2]$, $[(4a_1)^2(2e)^4(5a_1)^0(6a_1^*)^2]$, and $[(4a_1)^2(2e)^4(5a_1)^1(6a_1^*)^1]$ for SiH_4 and $[(2a_1)^2(1e)^4(3a_1)^2]$, $[(2a_1)^2(1e)^4(3a_1)^0(4a_1^*)^2]$, and $[(2a_1)^2(1e)^4(3a_1)^1(4a_1^*)^1]$ for CH_4. The numbers of configuration in the CI wave function are 138117 and 40716 for SiH_4 and CH_4, respectively. The number of the configurations is not reduced for CH_4, while for SiH_4 the perturbation selection is carried out by Rayleigh–Schrödinger BK method[19)] where the energy threshold is chosen to be 0.01 μhartree. As the result, the number is reduced to about 13000—23000.

For the dissociation limit the geometry optimization and the MR-SD-CI subsequent to the MCSCF calculation are also performed with the same basis set for SiH_3

and CH_3. The number of configuration in the MCSCF wave function is 2352, and that in the CI wave function is 16125 for CH_4 and 16103 for SiH_4 after the configuration selection.

The program Gaussian88[20] is employed for geometry optimization. The program employed for the UHF and the MCSCF calculations is HONDO7.[21] MELDF[22] is employed for the MR-SD-CI calculation.

Feature of the Geometry and the Minimum Energy Path Potential. The optimized geometries and total energies for the equilibrium states of SiH_4, SiH_3, CH_4, and CH_3 are shown in Table 1. SiH_3 is pyramidal while CH_3 is planar. These results are consistent with the experimental studies.[23] The optimized length r of SiH_4 is longer than that of CH_4 by 0.40 Å. The variations of r are very small during the reaction for both systems. The changes of the optimized angles ϕ as a function of R are shown in Fig. 2. The angles ϕ for SiH_4varies little because the geometry of the SiH_3 group does not change significantly along the reaction coordinate R, while that for CH_4 varies drastically because the CH_3 group changes from the pyramidal to the planar.

Table 1. Optimized Geometry and Total Energy of the Equilibrium States

Molecule	Symmetry	r	ϕ	Total energy
		Å	degree	hartree
SiH_4	T_d	1.4793	109.47	−291.411300
SiH_3	C_{3v}	1.4796	108.05	−290.769670
CH_4	T_d	1.0848	109.47	−40.397990
CH_3	D_{3h}	1.0760	90.00	−39.729275

Geometry optimization is performed at a UHF level with a DZP basis set. Total energy is calculated by the MC-SCF-CI method at the optimized geometry. The symbol r denotes the bond length of Si–H or C–H, and ϕ is the angle of H–Si···H or H–C···H.

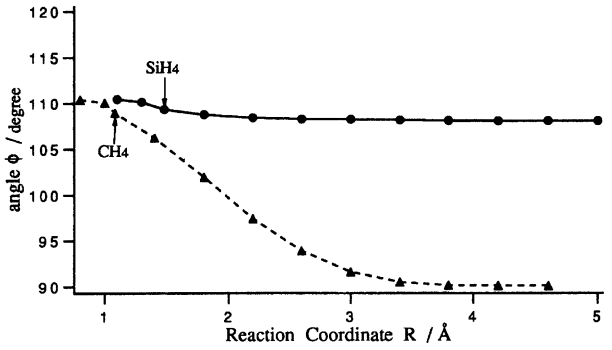

Fig. 2. The variation of the optimized angle ϕ for the SiH_4 and CH_4 systems as a function of the reaction coordinate R. ϕ is the angle between the C_3 axis and Si–H (C–H) bond of the $SiH_3(CH_3)$ group. The continuous line is for SiH_4 and the dashed line for CH_4. The arrows indicate the equilibrium points for both systems.

The minimum energy path potentials for the SiH_4 and CH_4 systems are shown in Fig. 3. Both are of non-barrier type. These ab initio potential energy curves are found to fit neither to the standard Morse nor the generalized Morse function. In the present work the minimum energy path potential is fitted to a spline interpolation function. This analytic function is used for fitting the free energy as will be described with relation to Eq. 13.

The dissociation energies obtained in the present ab initio calculation are 380.8 and 449.6 kJ mol^{-1} for the SiH_4 and CH_4 system, respectively. The experimental dissociation energies are 389 and 470 kJ mol^{-1} for SiH_4 and CH_4,[24,25] respectively. The calculated energies are smaller by 2.1 and 4.4% than the experimental energies.

Harmonic Analysis. The harmonic frequencies for the normal modes at the equilibrium geometries are listed in Table 2 along with the experimental values. They are computed by the direct diagonalization of the Cartesian force constants matrix that is obtained by the UHF/DZP procedure. The nine normal modes of the parent molecules of T_d symmetry are classified by regarding the dissociating Si–H or C–H bond as distinguishable from the other; a: doubly degenerate Si–H (C–H) stretching; b: symmetric Si–H (C–H) stretching; c: doubly degenerate in-plane bending; d: symmetric out-of-plane bending; e: doubly degenerate out-of-plane

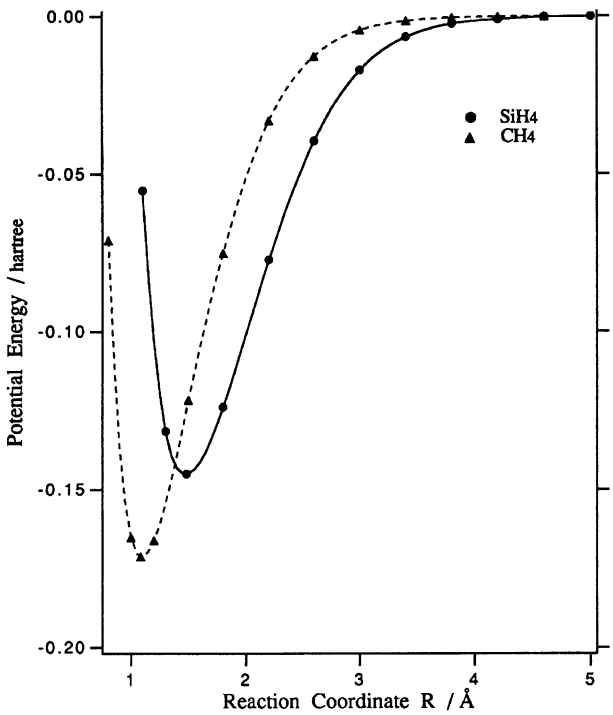

Fig. 3. The minimum energy path potential for the SiH_4 and CH_4 systems. The energy is calculated by the MCSCF-CI method with a DZP basis set at the optimized geometry for a given R. The circles and the triangles shows the calculated points. The lines are the curves fitted by the spline interpolation function.

Table 2. Vibrational Frequencies of the Equilibrium States

Molecule	Source	Vibrational frequency/cm^{-1}					
		a	b	c	d	e	f
SiH_4	experiment (Ref. 2)	2189	2189	972	913	913	2186
	this work	2337	2337	1054	1012	1012	2348
SiH_3	experiment (Ref. 2)	2161	2144	909	796	—	—
	this work	2335	2319	1016	874	—	—
CH_4	experiment (Ref. 7)	3154	3154	1573	1357	1357	3143
	this work	3294	3294	1670	1457	1457	3173
CH_3	experiment (Ref. 7)	3285	3270	1436	495	—	—
	this work	3445	3258	1518	405	—	—

Vibrational frequencies are obtained by the harmonic analysis at a UHF level with the C_{3v} symmetry. a: doubly degenerate Si–H (C–H) stretching, b: symmetric Si–H (C–H) stretching, c: doubly degenerate in-plane bending, d: symmetric out-of-plane bending, e: doubly degenerate out-of-plane bending, f: totally symmetric stretching. Here, "plane" means the plane defined by the three H-atoms of the SiH_3 or the CH_3 group.

bending; f: totally symmetric stretching. Here, "plane" means the plane defined by the three H atoms of the SiH_3 or CH_3 group.

The harmonic frequencies of the eight normal modes are also calculated along the minimum energy path. Here, the number of the normal modes is eight because the dissociative mode is excluded. The frequencies are obtained by the GF matrix method,[18,26] where the Cartesian force constant matrix is projected onto the internal force constant matrix for the eight internal coordinates excepting R. The eight normal modes are classified as follows; a: doubly degenerate Si–H (C–H) stretching of the $SiH_3(CH_3)$ group; b: symmetric Si–H (C–H) stretching of the $SiH_3(CH_3)$ group; c: doubly degenerate $SiH_3(CH_3)$ in-plane bending; d: symmetric $SiH_3(CH_3)$ out-of-plane bending; e: doubly degenerate $SiH_3\cdots H(CH_3\cdots H)$ bending. The variation of the frequencies as a function of the reaction coordinate is shown in Fig. 4.

For SiH_4, modes a, b, c, and d smoothly correlate to those of SiH_3 with the frequencies being little changed. For CH_4, the behavior of modes a, b, and c are similar to those of SiH_4 but the frequency of mode d diminishes drastically. This is because the weak resistance to the out-of-plane bending motion in the planar CH_3 leads to a much smaller force constant than that of the rigid pyramidal SiH_3.

For both systems the frequency of mode e approaches to zero at large R. This is reasonable because mode e correlates to the translation and rotation of the fragments of the dissociation. Therefore, it is crucial to treat the mode as a harmonic oscillator at large values of R. The motion should be described as the rotation of the dissociating H atom around the counterpart SiH_3 or CH_3 group at larger R. Such a motion will be more properly treated as an internal rotation hindered by the angular deformation potential. In Fig. 4 the results of both the hindered rotor (e_2) and the harmonic analyses (e_1) are shown. The procedure of the hindered rotor analysis is given in the following subsection.

Hindered Rotor Analysis. The two-dimensional hindered rotation is described by the two angles θ and ψ in Fig. 1.[7] The angular deformation potential can be obtained as a function of these angles at each R. The calculations for the potentials are carried out by the MR-SD-CI method with the same basis set and the reference configurations as in the calculation for the minimum energy path potential.

An example of the results is shown in Fig. 5, where the angular deformation potentials for the various values of angle ψ are described as a function of the angle θ. The values of R are fixed at 3.8 and 3.4 Å for SiH_4 and CH_4, respectively. The results show that the potential depends little on the angle ψ, which allows us to treat the rotation in terms of one-dimensional hindered rotor depending only on the angle θ.

The Schrödinger equation for a given R is given in Eq. 4.[17]

$$\left[-\frac{\hbar^2}{2I_{\text{eff}}}\left\{\frac{1}{\sin\theta}\frac{\partial}{\partial\theta}\left(\sin\theta\frac{\partial}{\partial\theta}\right)-\frac{M^2}{\sin^2\theta}\right\}+V(\theta)\right]\Theta_{\text{J,M}}(\theta) = E_{\text{J,M}}\Theta_{\text{J,M}}(\theta), \tag{4}$$

$E_{\text{J,M}}$ stands for the energy level of the hindered rotor. $V(\theta)$ is the potential of the one-dimensional hindered rotor. If $V(\theta)=0$, the equation becomes that for free rotors. The effective moment of inertia for the hindered rotor, I_{eff}, is obtained by the G-matrix.[26] For SiH_4 and CH_4, I_{eff} is written as below in the coordinate system of Fig. 1.

$$I_{\text{eff}} = \left[\frac{R^2+r^2-Rr(3-\cos^2\chi)}{R^2r^2\sin^2\chi}\frac{1}{m_{\text{A}}}+\frac{R^2+r^2}{R^2r^2}\frac{1}{m_{\text{H}}}\right]^{-1}. \tag{5}$$

In Eq. 5, $\cos\chi=\sin\theta\cos\psi\sin\phi+\cos\theta\cos\phi$ and m_{A} and m_{H} are the masses of SiH_4 or CH_4 and of the H-atom, respectively. Although I_{eff} depends on angle θ and ψ, the dependence is smaller enough so that I_{eff} may be regarded as a constant for a given R.

There are various models for the functional form of the hindering potential $V(\theta)$.[27] In the present work the following form is assumed;

$$V(\theta) = V(0)+\sum_{k=1}^{4} b_k \sin(k\theta). \tag{6}$$

Here, b_k is the fitting parameter. The potential curves fitted to this form are shown in Fig. 5. As an example of other models the sinusoidal curve proposed by Pacey[17] is also shown in Fig. 5. Since distortions of a large value of θ are not realistic in the thermal reaction, the fitting is carried out only up to 50° in Fig. 5. It is seen that the potential function in Eq. 6 agrees well with the results

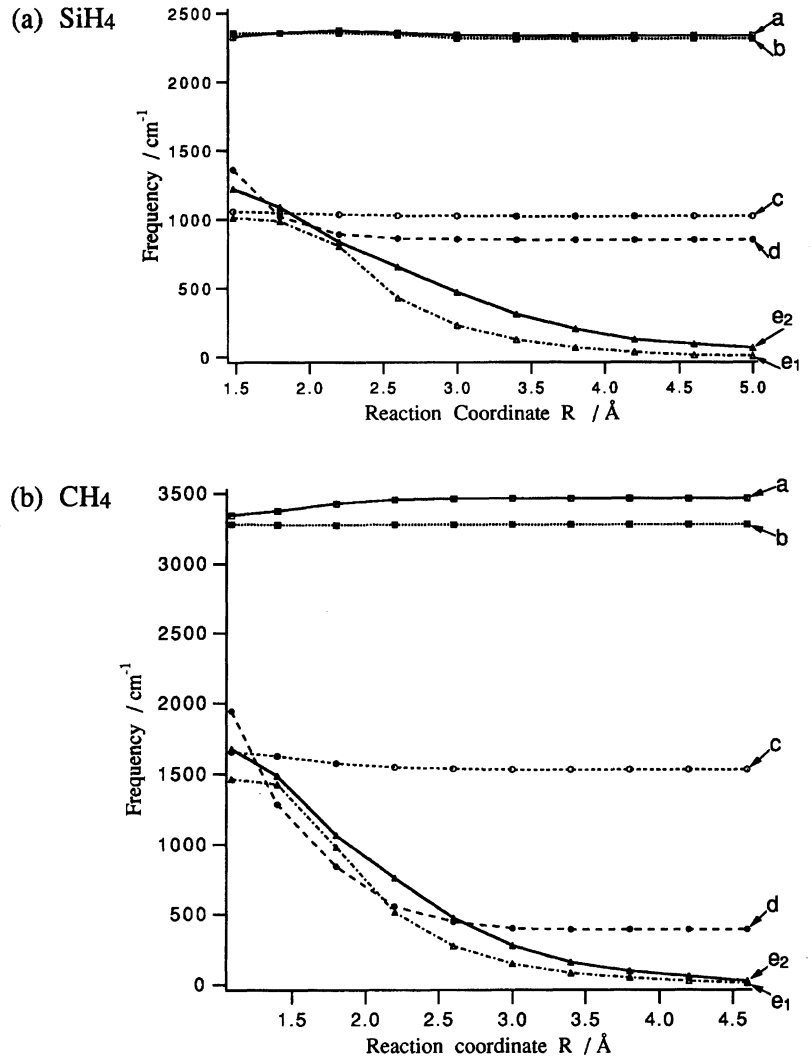

Fig. 4. The vibrational frequencies against the reaction coordinate for the SiH_4 and CH_4 systems. (a) for SiH_4 and (b) for CH_4. a: doubly degenerate Si–H (C–H) stretching of the $SiH_3(CH_3)$ group, b: symmetric Si–H (C–H) stretching of the $SiH_3(CH_3)$ group, c: doubly degenerate $SiH_3(CH_3)$ in-plane bending, d: symmetric $SiH_3(CH_3)$ out-of-plane bending, e_1: doubly degenerate $SiH_3\cdots H$ ($CH_3\cdots H$) bending (harmonic), e_2: doubly degenerate $SiH_3\cdots H$ ($CH_3\cdots H$) bending (hindered rotor). Here, "plane" means the plane defined by the three H atoms of the SiH_3 or CH_3 group. The results of a, b, c, d, and e_1 are for the harmonic analysis, while those of e_2 are for the hindered rotor analysis.

of the ab initio calculation in this range of θ but that the sinusoidal function does not. The standard deviations in fitting the curves for ψ=0°, 30°, and 60° by Eq. 6 are at most 0.00032 and 0.00034 for the equilibrium state of SiH_4 and CH_4, respectively. The deviations become smaller than 0.00001 in the region of the CVTST saddle points ($R \geq 3.0$ Å for SiH_4 and $R \geq 2.6$ Å for CH_4). Thus, the functional form is considered to be appropriate as the hindering potential for the CVTST calculation.

The eigenfunction of Eq. 4 is expanded in terms of the associated Legendre functions;[17]

$$\Theta_{J,M}(\theta) = \sum_{n=0}^{N-1} C_{n(J,M)} P_{n+N}^{M}(\theta), \qquad (7)$$

where N is the dimension of the expansion. Then, the one-dimensional hindered rotor equation is solved by the diagonalization of the N-dimensional Hamiltonian matrix.

To obtain the CVTST rate constant it is necessary to calculate the partition function. The partition function for the degenerate transitional bending mode is calculated as

$$q_{hr} = \sum_{J=0}^{N-1} \sum_{M=-J}^{+J} \exp\left[-(E_{J,M} - E_{0,0})/k_B T\right]. \qquad (8)$$

Here, $E_{J,M}$ is the eigenvalue of the hindered rotor and $E_{0,0}$ is the zero-point energy. Because of the calculational limitation in the diagonalization N in Eq. 7 is set to 20 and the eigenvalues for larger M and J are numerically extrapolated to N=50.[17] The contribution from these extrapolated energy levels in the partition function is almost zero at lower temperatures but it becomes significant at higher temperatures, that is, about 2.5 and 15% increase at 1000 and 2000 K for SiH_4 and

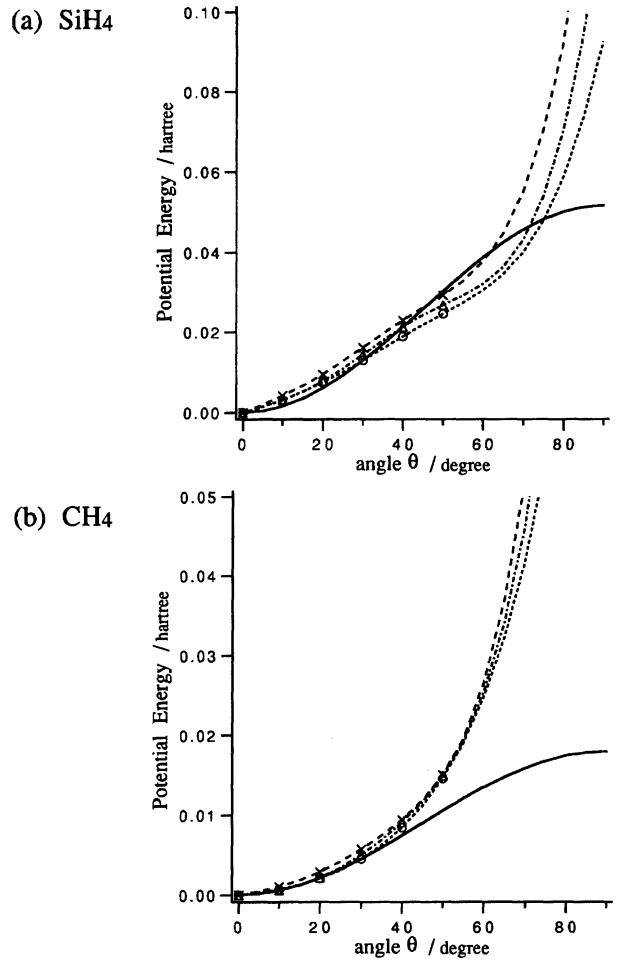

Fig. 5. The angular deformation potential as a function of the angle θ. (a): for SiH_4 at R=3.8 Å (b): for CH_4 at R=3.4 Å. ○, ×, △: the results of the calculation for ψ=0°, 30°, and 60°, respectively. —: sinusoidal function fitted for ψ=0°, ····: function in Eq. 6 fitted for ψ=0°, ---: function in Eq. 6 fitted for ψ=30°, –·–: function in Eq. 6 fitted for ψ=60°.

about 0.1 and 2.5% increase at the same temperatures for CH_4, respectively.

Calculation of Rate Constants

Method of Calculation. In CVTST the generalized rate constant for the association and dissociation reactions are expressed as

$$k(T,R) = \sigma \frac{k_B T}{h} \exp\left\{-\frac{\Delta G(T,R)}{k_B T}\right\} \quad (9)$$

$$\Delta G(T,R) = G(T,R) - G(T,\infty) \quad (10)$$

for the association and

$$\Delta G(T,R) = G(T,R) - G(T,R_0) \quad (11)$$

for the dissociation.[16] $G(T,R)$ and $G(T,\infty)$ are the free energy of the system at R and at the infinite separation whereas $G(T,R_0)$ is that of the parent molecules in the equilibrium state. The difference of the free energies $\Delta G(T,R)$ comprises the following seven components.

$$\frac{\Delta G(T,R)}{k_B T} = \frac{V_{MEP}(R)}{k_B T} - \Delta \ln Q_{trans}(T) - \Delta \ln Q_{rot}(T,R) + \frac{\Delta E_{zp,vib}(R)}{k_B T} + \frac{\Delta E_{zp,hr}(R)}{k_B T} - \Delta \ln q_{vib}(T,R) - \Delta \ln q_{hr}(T,R). \quad (12)$$

$V_{MEP}(R)$ is the ab initio potential energy along the minimum energy path with $V_{MEP}(\infty)$=0 for the association reaction and $V_{MEP}(R_0)$=0 for the dissociation. $\Delta \ln Q_{trans}(T)$ and $\Delta \ln Q_{rot}(T,R)$ are,respectively, the differences in the partition functions of the translation and rotation (including the symmetry number of rotation). The contributions by the eight vibrational freedoms are separated to the two classes; $\Delta \ln q_{vib}(T,R)$ and $\Delta E_{zp,vib}(R)$ are, respectively, the vibrational parts relative to the zero-point energy and the difference of the zero-point energy of the harmonic modes of a, b, c, and d; $\Delta \ln q_{hr}(T,R)$ and $\Delta E_{zp,hr}(R)$ are for mode e that correlates to the translation and rotation of the dissociating fragments.

$V_{MEP}(R)$ is calculated by the MR-SD-CI following the MCSCF method as described in the section of Potential Energy Surface. The translational and rotational partition functions are calculated by the standard method.[16] The rotational constants are obtained from the optimized geometry. The vibrational partition functions for modes a, b, c, and d are calculated by the standard method using the harmonic frequencies orthogonal to the reaction coordinate that are obtained in the subsection of Harmonic Analysis, while the results of the hindered rotor analysis are used for the transitional bending mode (mode e). The ab initio free energies in Eq. 12 are calculated from these components at various temperatures from 200 to 3000 K.

The symbol σ in Eq. 9 is the symmetry factor for the reaction about the electronic degeneracy; σ is 1/4 and unity for the association and dissociation, respectively. In the present formulation the symmetry number for the rotation is included in the rotational partition function. For the association reaction the ratio of the symmetry number of rotation is 3/3 between SiH_4 and SiH_3, whereas that for the CH_4 system is 3/6 due to the fact that CH_3 is of the D_{3h} symmetry in contrast to C_{3v} for SiH_4, SiH_3, and CH_4. For the dissociation reaction the ratios of the symmetry number of the rotation are unity for both systems at an arbitrary R and at the initial geometry.

The saddle point is determined by the maximum free energy criterion and the CVTST rate constant is defined as the generalized rate constant at the saddle point.[16] To determine the maximum point the calculated ab initio free energy at each temperature is fitted to the spline interpolation function in Eq. 13.

$$S(R_i \le R \le R_{i+1}) = G(R_i) + \sum_{k=1}^{3} C_{ik}(R - R_i)^k, \quad (13)$$

where $G(R_i)$ represents the point at which the free energy is calculated and C_{ik} is the interpolation coefficient.

Each curve is found to be smooth and shows a single peak, so the saddle point can be determined and the CVTST rate constants for the association and dissociation are calculated at this point for various temperatures.

Results of Calculation. The temperature dependence of the calculated saddle points and the CVTST rate constants for the SiH_4 and CH_4 systems are shown in Fig. 6, where the association and dissociation rate constants are given in units of 10^{10} l mol^{-1} s^{-1} and s^{-1}, respectively.

The decrease in R at the saddle point as the temperature increases is a common feature to barrierless association or dissociation reactions. The saddle points are at 4.6—3.3 Å and 3.8—2.7 Å for the SiH_4 and CH_4 system, respectively. At the same temperature the former is longer than the latter by 0.6—0.8 Å, which is larger than the difference in the length of Si–H and C–H in the equilibrium states, i.e., 0.4 Å. Thus, the SiH_4 system is considered to have a looser transition state than CH_4.

The association rate constant for SiH_4 is smaller than that for CH_4 by 4.0—6.0×10^{10} l mol^{-1} s^{-1} for all the temperatures studied and the difference at the same temperature amounts to 30—35% between the two systems. As shown in Fig. 6 (2) the association rate constants increase with the temperature first and then turn over at around 1600—2000 K. The slight decrease is interpreted as the result of the broken balance between the increase of the temperature and the increase of the free energy at higher temperatures. In this temperature region the association rate constants are regarded as essentially levelled-off.

As shown in Fig. 6 (3) the dissociation rate constants increase with the temperature. At the same temperature the dissociation rate constant for the SiH_4 system is always larger than for the CH_4 system; for example, the dissociation rate constant for the former system is larger by about one order of magnitude than for the latter at 2000 K, but the difference becomes smaller at higher temperatures.

Discussion

Free Energy and Its Components. The free energy and its components for the association and dissociation at various temperatures are listed in Table 3 along with the rate constants.

It is seen that the most important component for the dissociation is the potential energy part ($V_{MEP}(R)$). The dissociation rate constants are determined dominantly by the attractiveness of the minimum energy path potential. The association rate constants are expected to be sensitive to the shape of the minimum energy path potential in the region of larger R. In contrast to the dissociation other contributions such as the translational part ($\Delta\ln Q_{trans}(T)$), the rotational part ($\Delta\ln Q_{rot}(T,R)$), and the transitional bending part ($\Delta\ln q_{hr}(T,R)$ and $\Delta E_{zp,hr}(R)$) to the free energy are also significant in the association. The balance of the potential energy part and other main contributions determines the magnitude of the association rate constant.

The variation of the free energy and its components as a function of the reaction coordinate for the association at 500 K is shown in Fig. 7.

The location of the saddle point is determined by the variational rates of the components. Since the contribution of the harmonic vibrational part ($\Delta\ln q_{vib}(T,R)$ and $\Delta E_{zp,vib}(R)$) for the association is so small, it is neglected. The translational part is also negligible because it is constant against the temperature. Consequently, the major components which dictate the maximum point of the free energy curve are the potential energy part, the rotational part, and the transitional bending part. The transitional bending part is especially important because it gives a major negative contribution to the free energy and varies sensitively near the saddle point.

Comparison between the SiH_4 and CH_4 Systems. A remarkable difference between the SiH_4 and CH_4 systems is that SiH_3 is pyramidal while CH_3 is planar. The difference in the variation of the frequency and the vibrational partition function for mode d (symmetric $SiH_3(CH_3)$ out-of-plane bending mode) along the reaction coordinate occurs as the result of this geometrical difference; in the SiH_4 system the frequency of mode d remains almost constant along the reaction coordinate, while that in the CH_4 system becomes smaller as the geometry of the CH_3 group becomes planar (see Figs. 2 and 4); the vibrational partition function for mode d in the latter system is larger than that in the former system, and the difference becomes greater at lager R.

The free energy and its components at the saddle point given in Table 3 will be examined to compare the results of the calculated rate constants of the SiH_4 and CH_4 systems: For the association the differences of the components of the potential energy, the harmonic vibration, and the translation are relatively small between the two systems. The major components that lead to the difference in their rate constants are the rotational part ($\Delta\ln Q_{rot}(T,R)$) and the transitional bending partition function ($\Delta\ln q_{hr}(T,R)$). The negative contribution to the free energy of the rotational part in the CH_4 system is larger than that in the SiH_4, while that of the transitional bending partition function in the SiH_4 system is larger than that in the CH_4. The difference in the contribution of the former is larger than that of the latter, and it is concluded that the most effective component that determines the difference is the rotational part. The difference of the rotational part originates from the rotational constant. Therefore, the difference

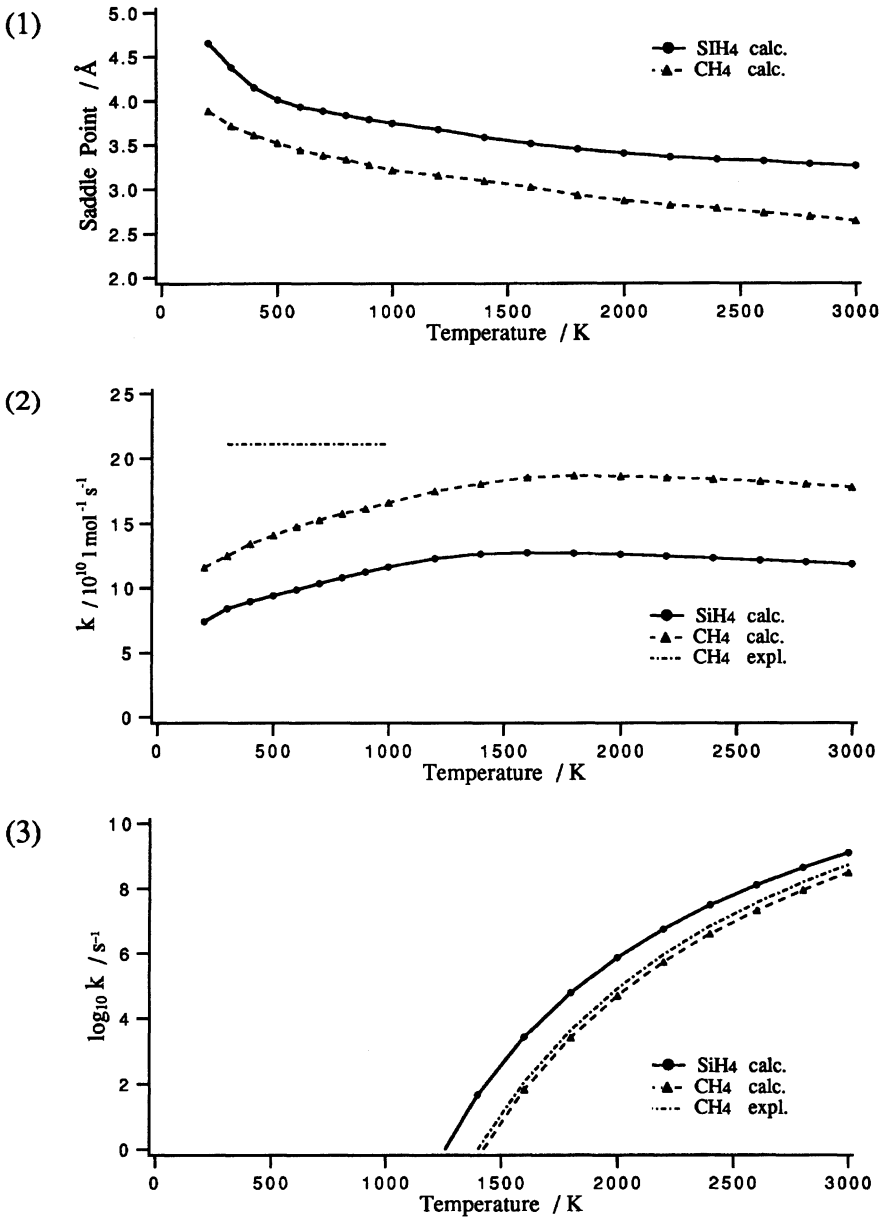

Fig. 6. The temperature dependence of the saddle point and the rate constants. (1) The temperature dependence of the saddle point in units of Å. (2) The temperature dependence of the association rate constant in units of 10^{10} $1\,mol^{-1}\,s^{-1}$. (3) The temperature dependence of the decimal logarithm of the dissociation rate constant in units of s^{-1}. The experimental rate constants for the CH_4 system shown in (2) and (3) are taken from Ref. 29.

in the association rate constant is governed practically by the difference in the molecular structures between the SiH_4 and CH_4 systems.

For the dissociation the component that affects the rate constants of the two systems most effectively is the potential energy part. The dissociation rate constant for the SiH_4 system exceeds that for the CH_4 because the minimum energy path potential is less attractive in the former system (see Fig. 3). At temperatures higher than 2000 K another important component to make the difference between the two systems sets in from mode d (included in $\Delta \ln q_{vib}(T,R)$ and $\Delta E_{zp,vib}(R)$). This is because their difference between the equilibrium state and the saddle point is large in the CH_4 system but small in the SiH_4 as described above.

Further difference between the two systems is the "tightness" of the transition state. As mentioned previously, the transition state of the SiH_4 system is looser than that of the CH_4 system by 0.2—0.3 Å at the same temperature. The reason for the difference is considered as due to the difference in the shape of the free energy curve as a function of the reaction coordinate; as shown in Fig. 7 the saddle point of the SiH_4 system is located on a smoother curve than the CH_4 system.

Comparison with Experimental and Other Theoretical Results. The accuracy of the calculated results of the SiH_4 system may be assessed by referring to the results of the CH_4 system for which abun-

Table 3. Free Energy and Its Components at the Saddle Point

(1) SiH_4					
Temp/K	300	500	1000	2000	3000
Saddle point/Å	4.38	3.90	3.74	3.40	3.26
Association rate constant $\times 10^{10}$/l mol^{-1} s^{-1}	8.4137	9.4007	11.6247	12.5167	11.8021
$\Delta G/k_BT$	6.1252	7.0359	8.2098	9.5262	10.3919
V_{MEP}/k_BT	−0.6905	−1.2167	−0.8926	−1.0523	−0.9816
$\Delta E_{zp,vib}/k_BT$	0.0000	0.0026	0.0013	0.0016	0.0021
$\Delta E_{zp,hr}/k_BT$	0.3598	0.4577	0.2887	0.2017	0.1559
$-\Delta \ln q_{vib}$	−0.0001	−0.0003	−0.0009	−0.0013	−0.0001
$-\Delta \ln q_{hr}$	−2.2526	−2.3829	−3.1616	−3.4783	−3.7159
$-\Delta \ln Q_{rot}$	−1.8500	−1.6601	−1.5936	−1.4466	−1.3836
$-\Delta \ln Q_{trans}$	10.5586	11.8357	13.5685	15.3014	16.3151
$\log_{10}$ of dissociation rate constant/s^{-1}	−49.4508	−23.5251	−3.9467	5.8605	9.1031
$\Delta G/k_BT$	143.3285	84.1431	39.7554	17.8665	10.8055
V_{MEP}/k_BT	151.9853	90.3887	44.9101	21.8490	14.2859
$\Delta E_{zp,vib}/k_BT$	−0.5635	−0.3355	−0.1677	−0.0828	−0.0542
$\Delta E_{zp,hr}/k_BT$	−4.4952	−2.4553	−1.1677	−0.5265	−0.3296
$-\Delta \ln q_{vib}$	−0.0100	−0.0405	−0.1028	−0.1566	−0.1773
$-\Delta \ln q_{hr}$	−2.2297	−2.2460	−2.6145	−2.2618	−2.0274
$-\Delta \ln Q_{rot}$	−1.3581	−1.1682	−1.1017	−0.9547	−0.8917
$-\Delta \ln Q_{trans}$	0.0	0.0	0.0	0.0	0.0
(2) CH_4					
Temp/K	300	500	1000	2000	3000
Saddle point/Å	3.71	3.52	3.25	2.87	2.64
Association rate constant $\times 10^{10}$l mol^{-1} s^{-1}	12.4967	14.0716	16.5622	18.5825	17.7546
$\Delta G/k_BT$	5.7296	6.6325	7.8559	9.1297	10.0121
V_{MEP}/k_BT	−0.9030	−0.8175	−0.7710	−1.0141	−1.2214
$\Delta E_{zp,vib}/k_BT$	0.0063	0.0062	0.0062	0.0162	0.0262
$\Delta E_{zp,hr}/k_BT$	0.4487	0.3410	0.2446	0.2065	0.1870
$-\Delta \ln q_{vib}$	0.0015	0.0041	0.0112	0.0818	0.2046
$-\Delta \ln q_{hr}$	−1.5062	−1.9526	−2.5562	−3.0198	−3.1888
$-\Delta \ln Q_{rot}$	−2.8268	−2.7348	−2.5980	−2.3926	−2.2610
$-\Delta \ln Q_{trans}$	10.5090	11.7861	13.5190	15.2518	16.2655
$\log_{10}$ of dissociation rate constant/s^{-1}	−59.7782	−29.6457	−6.8195	4.6861	8.4810
$\Delta G/k_BT$	167.1083	98.2364	46.3704	20.5705	12.2379
V_{MEP}/k_BT	179.4978	107.4229	53.3491	26.0459	16.8186
$\Delta E_{zp,vib}/k_BT$	−2.6033	−1.5596	−0.7767	−0.3752	−0.2346
$\Delta E_{zp,hr}/k_BT$	−6.5408	−3.8527	−1.8521	−0.8418	−0.5119
$-\Delta \ln q_{vib}$	−0.1525	−0.3624	−0.7201	−0.9442	−0.9365
$-\Delta \ln q_{hr}$	−1.5035	−1.9143	−2.2692	−2.1589	−1.8740
$-\Delta \ln Q_{rot}$	−1.5893	−1.4974	−1.3605	−1.1551	−1.0235
$-\Delta \ln Q_{trans}$	0.0	0.0	0.0	0.0	0.0

Free energy and its components are given non-dimensionally.

dant experimental information is available. The association rate constant of the CH_4 system calculated in the present work are compared with available experimental and other theoretical results in Table 4.[4—6,11—15]

The three experimental values are rather widely scattered perhaps because of the difference in the experimental methods. However, the average of the experimental constants at 300 K agree with the result in the present work.

The present results are also inbetween other theoretical results which include the CVTST method on the basis of the DHS potential surface (a stiff Morse function for the C–H stretching),[11] the same method on the basis of the modified DHS potential surface (fitted to the Hirst potential surface[28]),[12] the flexible microcanonical variational transition state theory based on the same potential surface as Ref. 12,[13] the classical trajectory method on the basis of the another modified DHS potential surface,[14] and the statistical adiabatic channel model on the basis of the Hirst potential surface.[15]

The results in Refs. 11 and 12 should be more appropriate for the comparison with the present work in

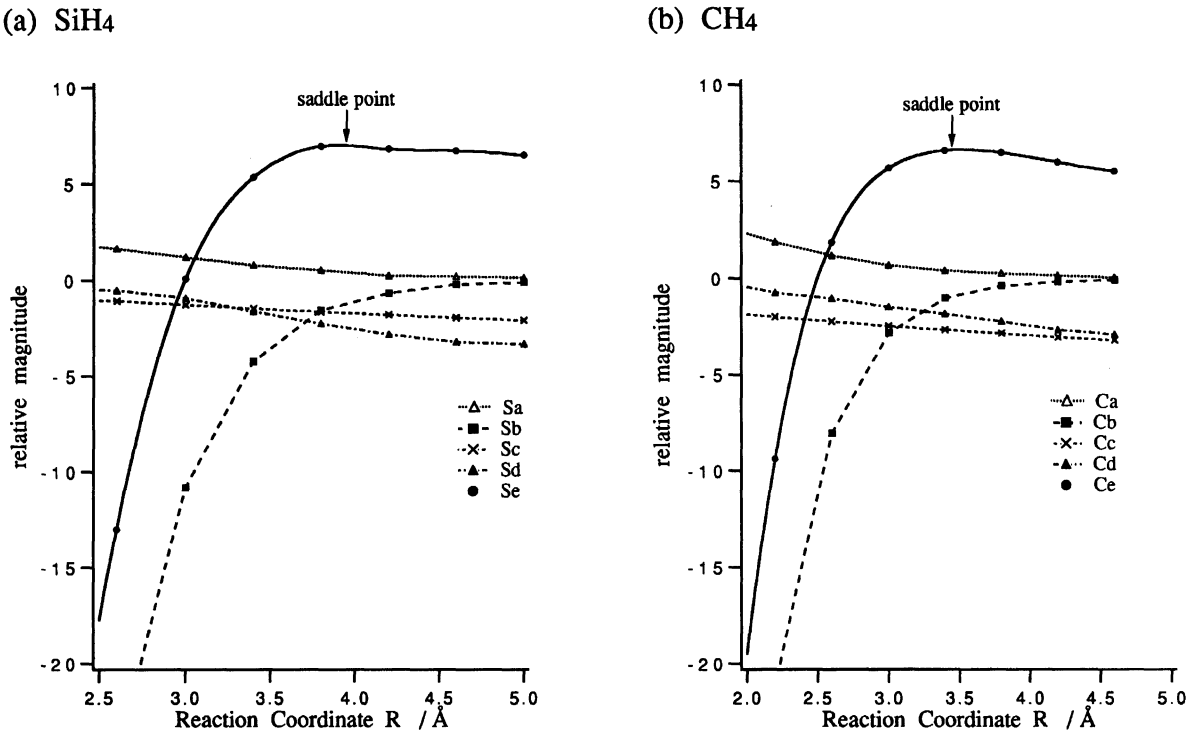

Fig. 7. The variation of the free energy and its components at 500 K for the association reaction. (a) for SiH_4 and (b) for CH_4. Sa, Ca: $E_{zp,hr}/k_BT$; Sb, Cb: V_{MEP}/k_BT; Sc, Cc: $-\Delta \ln Q_{rot}$; Sd, Cd: $-\Delta \ln Q_{hr}$; Se, Ce: $\Delta G/k_BT$. The contribution of the harmonic vibration is small enough to be neglected. The translational partition function is constant against the temperature, so it is also neglected. Se and Ce are fitted to the spline interpolation function in Eq. 13. In this caption S and C stand for SiH_4 and CH_4, respectively.

Table 4. Comparison with Experimental and Other Theoretical Results for the Association Rate Constant of CH_4 System

Method	Source	Rate constant $\times 10^{10}$/l mol^{-1} s^{-1}			
		300 K	500 K	1000 K	2000—2200 K
Experiment 1	Ref. 4	20.0±9.0			
Experiment 2	Ref. 5	12.0±3.0			
Experiment 3	Ref. 6	9.0±4.0			
CVTST[a)]	Ref. 11	7.6	9.2	11.0	11.2
CVTST[b)]	Ref. 12	15.9	18.4	21.2	—
FμVTST[c)]	Ref. 13	14.2	17.3	20.6	21.5
Trajectory[d)]	Ref. 14	13.7	—	20.5	20.7
SACM[e)]	Ref. 15	6.5	8.0	10.0	12.5
CVTST	This work	12.5	14.1	16.6	18.6

a) Canonical VTST on the Duchovic–Hase–Schlegel potential surface, b) Canonical VTST on the modified Duchovic–Hase–Schlegel potential surface, c) Flexible microcanonical VTST on the modified Duchovic–Hase–Schlegel potential surface, d) Classical trajectory method on the modified Duchovic–Hase–Schlegel potential surface, e) Statistical adiabatic channel model on the Hirst potential surface.

more detail because both are based on CVTST as in the present work. The difference among the three CVTST approaches are in the difference of the potential energy surfaces employed. Among the three the difference in the translational, the rotational, and the harmonic vibrational parts of the free energy is considered to be small. One cause of the difference in the association rate constant among the three may be the difference in the shape of the minimum energy path potential at larger R region; the minimum energy path potentials in Refs. 11 and 12 are obtained on the basis of the stiff Morse function fitted to an ab initio C–H stretching potential that is calculated at the MP4/6-31G** and the MRD-CI/6-31G** levels, respectively. Another cause may be the difference in the treatment of the transitional bending mode; the mode is treated as a quantum

mechanical hindered rotation in Ref. 11 with the sinusoidal approximation to the hindering potential, while it is treated as the classical hindered rotation in Ref. 12. The result by the former treatment is compared with the present result in Fig. 5 and discussed in the subsection of Hindered Rotor Analysis; the sinusoidal approximation gives poor results at lager θ. The treatment in terms of the classical hindered rotation is compared with the present treatment (see Table 5); the saddle points in Ref. 12 are shorter and the transitional bending partition functions in Ref. 12 are larger than those in the present work. The larger partition function leads to the tighter transition state and the smaller free energy to give the lager association rate constant of 15.9×10^{10} $\mathrm{l\,mol^{-1}\,s^{-1}}$ (see Table 4).

From Table 3 it is seen that the association rate constant for the SiH_4 system obtained in the present work is smaller than that for the CH_4 by $4.0—6.0\times10^{10}$ $\mathrm{l\,mol^{-1}\,s^{-1}}$, or percentagewise, 30—35% at the same temperature. As mentioned previously, the difference mainly originates from the difference in the molecular structures of SiH_4 and CH_4. Thus, the difference between the two systems may not depend critically upon the calculational method. The association rate constant obtained in the present work should be useful for the prediction of the thermal rate constant for the SiH_4 system.

For the dissociation the attractive character of the potential energy surface affects sensitively the rate constant. The experimental dissociation energies are larger than those of the present ab initio potential energies of both SiH_4 and CH_4 systems (see the section of Potential Energy Surface). Thus, the real dissociation rate constants are expected to be a little smaller than those obtained in the present work. They are evaluated by substituting the value of the experimental dissociation energy to the minimum energy path potential; the results are 2—3% and 5—6% for the SiH_4 and CH_4 system, respectively, in the scale of the decimal logarithm.

A recent comprehensive review of the experimental rate constants of the reactions $CH_4 \rightleftarrows CH_3+H$ recommends the following values for the forward and the backward reactions, respectively.[29]

$$k_{\mathrm{expl}}(\mathrm{dissoc.}) = (2.4\times10^{16})\exp(-52800/T)\ \mathrm{s^{-1}},$$
$$T = 1000—3000\ \mathrm{K}$$
$$k_{\mathrm{expl}}(\mathrm{assoc.}) = 21.1\times10^{10}\ \mathrm{l\ mol^{-1}s^{-1}},$$
$$T = 300—1000\ \mathrm{K}.$$

Since the accuracy of the experimental values is said to be $\Delta\log k_{\mathrm{expl}}(\mathrm{dissoc.})=\pm0.5$ and $\Delta\log k_{\mathrm{expl}}(\mathrm{assoc.})=\pm0.3$ in the cited reference, the present results of $k_{\mathrm{calc}}(\mathrm{dissoc.},\ 2000\ \mathrm{K}) = 4.85\times10^4\ \mathrm{s^{-1}}$, i.e., $\log k_{\mathrm{calc}}(\mathrm{dissoc.},\ 2000\ \mathrm{K}) = 4.69$ and $k_{\mathrm{calc}}(\mathrm{assoc.},\ 300\ \mathrm{K}) = 12.5\times10^{10}\ \mathrm{l\,mol^{-1}\,s^{-1}}$, i.e., $\log k_{\mathrm{calc}}(\mathrm{assoc.},\ 300\ \mathrm{K}) = 11.10$ are well within the error of the experimental values, i.e., $\log k_{\mathrm{expl}}$ (dissoc., 2000 K)$=4.92\pm0.5$ and $\log k_{\mathrm{expl}}$ (assoc., 300 K)$=11.32\pm0.3$.

Table 5. Comparison of Hindered Rotor Partition Function

Temp	Ref.12 Saddle point	q_{hr}	This work Saddle point	q_{hr}
K	Å		Å	
300	3.55	4.878	3.71	4.509 (4.053)
500	3.37	7.548	3.52	7.047 (6.325)
800	3.17	10.723	3.33	10.533 (10.107)
1000	3.07	12.578	3.25	12.886 (12.161)

The value of the transitional bending partition function at each saddle point is designated. The value in parentheses is for the partition function at the counterpart saddle point of Ref. 12.

Conclusion

In this paper the thermal rate constants for $SiH_4 \rightleftarrows SiH_3+H$ and $CH_4 \rightleftarrows CH_3+H$ reactions are calculated on the basis of the ab initio potential energy surface and the CVTST method. The minimum energy path potentials are calculated by the MR-SD-CI followed by the MCSCF method with the Huzinaga–Dunning plus polarization (DZP) basis set. The harmonic frequencies for the normal modes orthogonal to the reaction coordinate are calculated by the UHF/DZP level. The transitional bending mode is treated ad hoc as a quantum mechanical two-dimensional hindered rotor.

The results are summarized as below:

(1) The association rate constant for the CH_4 system is favorably comparable with experimental and other theoretical results. The association rate constant for the SiH_4 system is predicted to be smaller than that for the CH_4 by $4.0—6.0\times10^{10}$ $\mathrm{l\,mol^{-1}\,s^{-1}}$, or percentagewise, 30—35% at the same temperature.

(2) The association rate constants are determined by the balance of the potential energy, the translational, the rotational and the transitional bending parts of the free energy. The difference between the SiH_4 and CH_4 systems mainly originates from the difference in the rotational part as a result of the difference in the molecular structure of SiH_4 and CH_4.

(3) The dissociation rate constants depend mainly on the attractiveness of the minimum energy path potential. The vibrational component that contributes significantly to the difference between the SiH_4 and CH_4 systems is mode d (the symmetric $SiH_3(CH_3)$ out-of-plane bending mode). The difference in mode d is attributed to the difference in the molecular geometries in the dissociation limit, i.e., pyramidal SiH_3 and planar CH_3.

(4) The real dissociation rate constants are evaluated to be 2—3% and 5—6% smaller in the decimal logarithm scale for the SiH_4 and CH_4 system, respectively, than those calculated in the present work.

(5) The location of the saddle point is determined mainly by the transitional bending mode. The SiH_4 system has a looser transition state than the CH_4 system. The saddle point of the former is longer than that of the latter at the same temperature by 0.6—0.8 Å.

The authors are grateful to Professor Shigeki Kato for his valuable comments and discussions. Dr. Nobuaki Washida and Dr. Akira Miyoshi kindly provided them pertinent information of the kinetics of the system studied. Numerical calculations were performed at the Computer Center of the Kyoto University and IMS Computer Center. The study was partially supported by Grants-in-Aid for Scientific Research on Priority Areas Nos. 0424203, 05233108, and 05237106.

References

1) P. Ho, W. G. Breiland, and M. E. Coltrin, "Silicon Chemistry," Chap. 37.
2) P. Ho, M. E. Coltrin, J. S. Binkley, and C. F. Melius, *J. Phys. Chem.*, **89**, 4647 (1985).
3) R. Viswanathan, D. L. Thompson, and L. M. Raff, *J. Chem. Phys.*, **80**, 4230 (1984).
4) J. Cheng and C. Yeh, *J. Phys. Chem.*, **81**, 1982 (1977).
5) T. J. Sworski, C. J. Hochanadel, and P. J. Ogren, *J. Phys. Chem.*, **84**, 129 (1980).
6) R. Patrick, M. J. Pilling, and G. J. Rogers, *Chem. Phys.*, **53**, 279 (1980).
7) R. J. Duchovic, W. L. Hase, and H. B. Schlegel, *J. Phys. Chem.*, **88**, 1339 (1984).
8) R. J. Duchovic and W. L. Hase, *Chem. Phys. Lett.*, **110**, 474 (1984).
9) R. J. Duchovic and W. L. Hase, *J. Chem. Phys.*, **82**, 3599 (1985).
10) W. L. Hase and R. J. Duchovic, *J. Chem. Phys.*, **83**, 3448 (1985).
11) J. F. LeBlanc and P. D. Pacey, *J. Chem. Phys.*, **83**, 4511 (1985).
12) W. L. Hase, S. L. Mondro, R. J. Duchovic, and D. M. Hirst, *J. Am. Chem. Soc.*, **109**, 2916 (1987).
13) E. E. Aubanel and D. M. Wardlaw, *J. Phys. Chem.*, **93**, 3117 (1989).
14) X. Hu and W. L. Hase, *J. Chem. Phys.*, **95**, 8073 (1991).
15) C. J. Cobos, *J. Chem. Phys.*, **85**, 5644 (1986).
16) a) A. D. Isaacson and D. G. Truhlar, *J. Chem. Phys.*, **76**, 1380 (1982); b) S. N. Rai and D. G. Truhlar, *J. Chem. Phys.*, **79**, 6046 (1983).
17) P. D. Pacey, *J. Chem. Phys.*, **77**, 3540 (1982).
18) M. Aoyagi and S. Kato, *J. Chem. Phys.*, **88**, 6409 (1988).
19) D. Rawlings and E. R. Davidson, *Chem. Phys. Lett.*, **98**, 424 (1983).
20) IMS version of program Gaussian82.
21) M. Dupuis et al., HONDO: Version 7.0 (1987) QCPE 544.
22) E. R. Davidson et al., Quantum Chemistry Group, Indiana University (1988) QCPE 580.
23) R. Jans and R. G. A. R. Maclagan, *Aust. J. Chem.*, **37**, 2159 (1984).
24) A. M. Doncaster and R. Walsh, *Int. J. Chem. Kinet.*, **13**, 503 (1981).
25) S. P. Heneghan, P. A. Knoot, and S. W. Benson, *Int. J. Chem. Kinet.*, **13**, 677 (1981).
26) E. B. Wilson, J. C. Decius, and P. C. Cross, "Molecular Vibrations," McGraw-Hill, New York (1955).
27) M. J. T. Jordan, S. C. Smith, and R. G. Gilbert, *J. Phys. Chem.*, **95**, 8685 (1991).
28) D. M. Hirst, *Chem. Phys. Lett.*, **122**, 225 (1985).
29) D. L. Baulch, C. J. Cobos, R. A. Cox, C. Esser, P. Frank, Th. Just, J. A. Kerr, M. J. Pilling, J. Troe, R. W. Walker, and J. Warnatz, *J. Chem. Phys. Ref. Data*, **21**, 411 (1992).